Saturated Liquid Densities of HCFC 123 and HFC 134a

Yukishige Maezawa,* Haruki Sato, and Koichi Watanabe

Department of Mechanical Engineering, Faculty of Science and Technology, Keio University, Yokohama 223, Japan

Saturated liquid densities of HCFC 123 and HFC 134a were measured by a magnetic densimeter. The results cover the range of temperatures from 200 to 400 K or the critical temperature. Vapor pressures and compressed liquid densities were also measured from 280 to 350 K in temperature and from 0.5 to 2.0 MPa in pressure. The experimental uncertainties for temperature, pressure, and density were estimated to be not greater than ±15 mK, ±7 kPa, and ±0.2%, respectively. The simple correlations for saturated liquid density of HCFC 123 and HFC 134a were developed.

Introduction

Recently, the ozone depletion and global warming by some CFCs, such as CFC 11, 12, 113, 114, and 115, have been becoming a worldwide issue. HCFC 123 (1,1-dichloro-2,2,2-trifluoroethane, $CHCl_2CF_3$) and HFC 134a (1,2,2,2-tetrafluoroethane, CH_2FCF_3) are expected as prospective substitutes for CFC 11 (trichloromonofluoromethane, CCl_3F) and CFC 12 (dichlorodifluoromethane, CCl_2F_2), respectively, because they contain the hydrogen atom and have short atmospheric lives, and therefore they have low ozone depletion potentials and low global warming potentials. This paper reports measured saturated liquid densities, vapor pressures, and compressed liquid *PVT* properties of these substances. These data would contribute to encouraging the basic design of advanced energy-conversion systems such as the organic Rankine or reversed Rankine cycle systems with environmentally acceptable refrigerants.

Experimental Section

All measurements of the present study were made by using a magnetic densimeter coupled with a variable volume cell. The present magnetic densimeter is essentially similar to the one developed by Okada et al. (*1*). The magnetic densimeter consists of a magnetic buoy, a sample cell, an electromagnetic coil, and a positioner as shown in Figure 1. A permanent magnet-mounted buoy (A) is made of Pyrex glass, which has an 8-mm outer diameter and a 30-mm length. A sample cell (C) is made of Pyrex glass so as to permit a direct observation of the position of the buoy and the meniscus (vapor–liquid boundary surface) of the sample. The buoy is immersed in a sample liquid and is lifted by an electromagnetic force generated by the electromagnetic coil (D) to a certain level where the Pyrex glass positioner (B) is located. During the measurements, detachment of the magnetic buoy from the positioner in the cell is detected to find the balancing point of the buoyancy with the electromagnetic force. The DC current through the electromagnetic coil is slowly reduced, and just when the buoy detaches from a certain positioner level, the following relationship among the forces is established:

$$F = m_B g - \rho V_B g = kI \qquad (1)$$

where F denotes the electromagnetic force, which is expressed by a product of a coil constant k and current I; m_B and V_B denote the mass and volume of the buoy, respectively; g denotes gravitational acceleration; and ρ is the sample liquid density. On the other hand, in the case of the buoy installed in a vacuum, the force balance is expressed as

$$F_V = m_B g = kI_V \qquad (2)$$

where subscript V denotes the value in vacuum. Combining eqs 1 and 2, the sample liquid density is given by

$$\rho = \rho_B(1 - I/I_V) \qquad (3)$$

where ρ_B ($=m_B/V_B$) denotes a density of the buoy. Accordingly, the sample liquid density is obtained by measuring the set of currents I and I_V in cases of the sample liquid and of vacuum, respectively, at each temperature.

A detachment of the buoy from the positioner is detected by using a search coil (E). When the buoy starts to fall from the positioner, an induced pulse current I_2 appears in the search coil. It should be noted that the coil current has been reduced slowly enough so as to eliminate the influence of time lag in the present measurements of fluorocarbon refrigerants, which generally have low viscosity.

Figure 2 shows a complete setup of the present apparatus. In the case of *PVT* measurements, the sample pressure was kept at a desired pressure by regulating the pressure of nitrogen gas filled outside the metallic bellows in the variable volume cell (B). The sample pressure was determined by calibrating the pressure difference between the sample and nitrogen gas in advance. The nitrogen gas pressure was measured by a precision digital pressure gauge (F; Heise Model 901B), whereas the pressure difference was measured by a differential pressure gauge (C; Validyne Model DP15-42). The sample temperature was measured by a 25-Ω standard platinum resistance thermometer (T) placed in the vicinity of the cell in a thermostated liquid bath (E).

The experimental uncertainty in temperature was estimated to be not greater than ±15 mK as a sum of 2 mK, the precision of the thermometer; 1 mK, the accuracy of the thermometer bridge; and 12 mK, the fluctuation of the thermostated liquid in the bath. The uncertainty in pressure was estimated to be not greater than ±7 kPa as a sum of 5 kPa, the accuracy of the pressure gauge, and 2 kPa, the accuracy of the differential pressure gauge. The uncertainty in density was estimated to be not greater than ±0.2% as a reproducibility of the magnetic densimeter. The purity of the sample used was 99.93 wt % for HCFC 123 and 99.99 wt % for HFC 134a.

Results

Saturated liquid densities were measured in wide ranges of temperatures from 200 to 400 K for HCFC 123 and from 200 to 370 K for HFC 134a; 23 and 25 data points were obtained for HCFC 123 and HFC 134a, respectively. Vapor pressures were measured at temperatures from 280 to 350 K for both fluids; 8 and 13 data points were obtained for HCFC 123 and HFC 134a, respectively. Compressed liquid *PVT* properties were measured in the ranges of temperatures from 280 to 340 K and of pressures from 0.5 (or vapor pressure) to 2.0 MPa for

* To whom correspondence should be addressed.

0021-9568/90/1735-0225$02.50/0

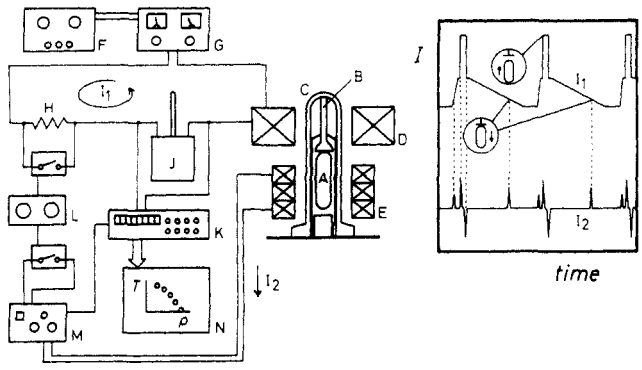

Figure 1. Magnetic densimeter: (A) magnetic buoy; (B) positioner; (C) pyrex glass cell; (D) electromagnetic coil; (E) search coil; (F) electric current controller; (G) precision dc power supply; (H) resistor; (J) standard resistor; (K) precision digital multimeter; (L) timer; (M) peak detector; (N) personal computer.

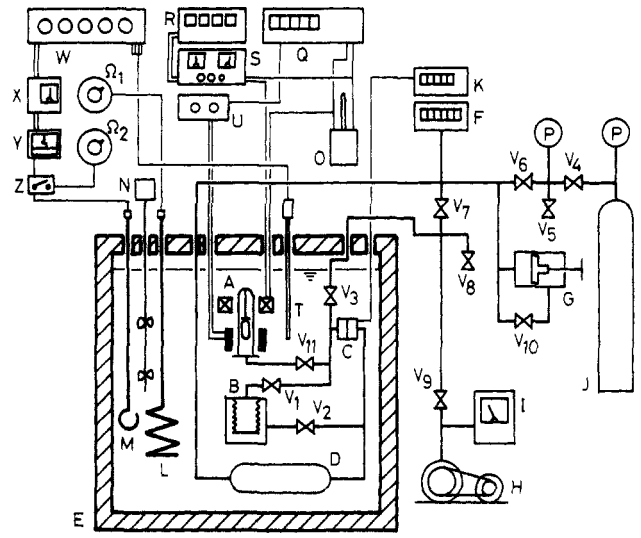

Figure 2. Experimental apparatus: (A) magnetic densimeter; (B) variable volume cell; (C) differential pressure gage; (D) damper; (E) thermostat; (F) precision digital pressure gauge; (G) precision pressure controller; (H) vacuum pump; (I) vacuum gauge; (J) nitrogen gas bomb; (K) differential pressure amplifier; (L) main heater or cooler; (M) subheater; (N) stirrer; (O) standard resistor; (P) pressure gauge; (Q) precision digital multimeter; (R) electric current controller; (S) precision dc power supply; (T) platinum resistance thermometer; (U) peak detector; (V_1–V_{11}) valve; (W) precision thermometer bridge; (X) galvanometer; (Y) pen recorder; (Z) microswitch; (Ω) transformer.

Table I. Saturated Liquid Densities of HCFC 123

no.	T/K	ρ/(kg·m^{-3})	no.	T/K	ρ/(kg·m^{-3})
1	200.001	1690.6	13	300.014	1456.2
2	210.012	1667.0	14	310.000	1430.9
3	219.999	1641.2	15	320.000	1404.6
4	229.991	1622.2	16	330.004	1377.9
5	230.001	1621.6	17	339.999	1349.8
6	240.066	1597.6	18	349.999	1321.0
7	250.003	1575.4	19	360.012	1287.4
8	260.001	1550.0	20	369.999	1257.3
9	269.970	1527.4	21	379.996	1222.1
10	270.010	1527.4	22	389.971	1190.4
11	279.969	1505.9	23	399.987	1144.7
12	289.988	1481.2			

Table II. Vapor Pressures of HCFC 123

no.	T/K	P/MPa	no.	T/K	P/MPa
1	279.969	0.046	5	320.000	0.192
2	289.988	0.067	6	330.004	0.253
3	300.014	0.097	7	339.999	0.338
4	310.000	0.136	8	349.999	0.440

Table III. Compressed Liquid Densities of HCFC 123

no.	T/K	P/MPa	ρ/(kg·m^{-3})
1	280.050	0.502	1507.9
2	280.030	0.997	1509.0
3	279.999	1.494	1510.0
4	279.877	1.996	1510.8
5	300.018	0.501	1456.6
6	300.039	0.998	1458.0
7	299.988	1.505	1459.5
8	300.018	2.001	1460.7
9	319.987	0.508	1404.8
10	319.988	0.996	1406.7
11	319.987	1.495	1408.6
12	319.987	2.000	1410.3
13	339.997	0.498	1349.7
14	339.999	0.999	1352.5
15	339.999	1.504	1354.9
16	339.999	2.001	1357.3

Table IV. Saturated Liquid Densities of HFC 134a

no.	T/K	ρ/(kg·m^{-3})	no.	T/K	ρ/(kg·m^{-3})
1	199.961	1506.3	14	300.009	1198.0
2	210.002	1479.7	15	309.987	1159.1
3	219.999	1451.2	16	310.052	1158.6
4	230.011	1422.2	17	319.988	1115.4
5	239.996	1395.0	18	319.991	1115.4
6	250.013	1364.4	19	330.007	1068.8
7	260.001	1334.4	20	330.007	1068.1
8	270.000	1303.0	21	340.025	1014.4
9	279.936	1270.5	22	349.989	949.8
10	280.004	1269.3	23	350.014	949.1
11	289.954	1235.5	24	359.991	868.4
12	289.978	1234.5	25	369.999	746.7
13	299.976	1198.7			

Table V. Vapor Pressures of HFC 134a

no.	T/K	P/MPa	no.	T/K	P/MPa
1	279.936	0.378	8	310.052	0.934
2	280.004	0.369	9	319.988	1.219
3	289.954	0.515	10	319.991	1.217
4	289.978	0.519	11	330.007	1.558
5	299.976	0.699	12	340.025	1.967
6	300.009	0.701	13	349.989	2.459
7	309.987	0.934			

Table VI. Compressed Liquid Densities of HFC 134a

no.	T/K	P/MPa	ρ/(kg·m^{-3})
1	279.857	0.505	1270.7
2	279.928	0.998	1272.4
3	279.999	1.493	1274.0
4	279.999	1.991	1275.7
5	300.017	0.978	1199.4
6	300.017	1.481	1202.3
7	300.017	1.982	1205.0
8	320.024	1.493	1117.1
9	320.024	1.989	1121.9
10	340.020	1.998	1014.3

both fluids; 16 and 10 data points were obtained for HCFC 123 and HFC 134a, respectively.

All measured data are given in Tables I–VI.

Discussion

The saturated liquid densities were correlated as a simple function of temperature as follows:

$$\rho'_r = 1 + A(1 - T_r)^a + B(1 - T_r)^b,$$

$$\rho'_r = \rho'/\rho_c, \quad T_r = T/T_c \tag{4}$$

where ρ' and T denote saturated liquid density and temperatures and ρ_c and T_c are the critical density and the critical temper-

Table VII. Critical Parameters and Coefficients of Equation 4

substance	T_c/K	ρ_c/(kg·m^{-3})	A	a	B	b
HCFC 123	456.86	556	2.236	0.368	0.5142	1.43
HFC 134a	374.30	508	2.451	0.38	0.4403	1.6

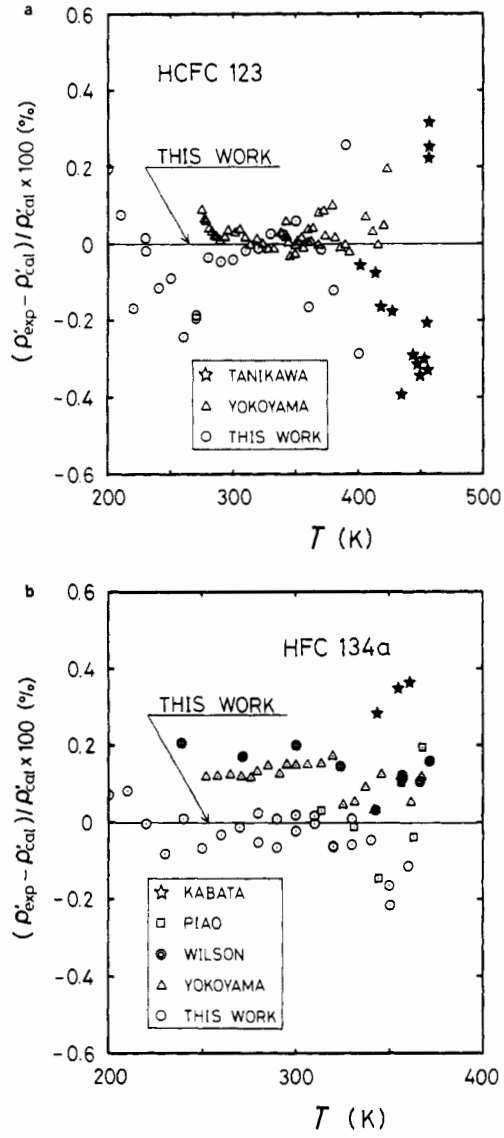

Figure 3. (a) Saturated liquid density deviations from eq 4 for HCFC 123. (b) Saturated liquid density deviations from eq 4 for HFC 134a.

ature, respectively. A, a, B, and b are adjustable parameters. A set of two exponents, a and b, was determined by trial and error, while the two coefficients, A and B, were determined by least-squares method. The critical parameters measured by Tanikawa et al. (*3*) for HCFC 123 and by Kabata et al. (*8*) for HFC 134a were used in the present study. The data used to develop the correlations were a total of 88 points for HCFC 123, including the present 23 data, 19 points reported by Tanikawa et al. (*3*), and 46 points reported by Yokoyama et al. (*2*), and a total of 32 points for HFC 134a, including the present 25 data and 7 points reported by Piao et al. (*4*). The numerical values of these parameters are given in Table VII. Exponents a and b for HCFC 123 have more figures than those for HFC 134a because the data at high temperatures reported by Tanikawa et al. (*3*) were included in the input data for correlating HCFC 123. Standard deviations of parameters A and B were

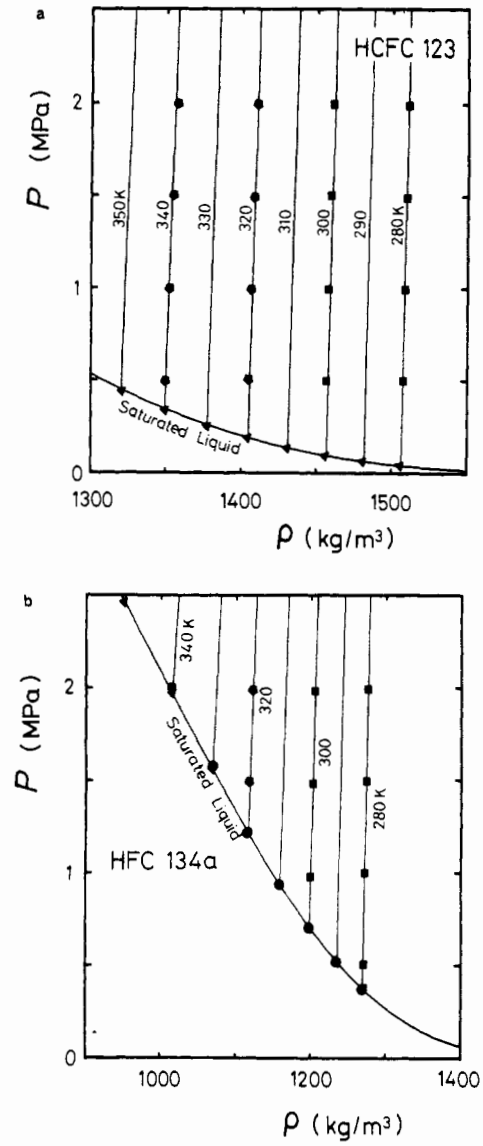

Figure 4. (a) Pressure–density diagram for HCFC 123. (b) Pressure–density diagram for HFC 134a.

±0.002 and ±0.0074 for HCFC 123 and ±0.003 and ±0.0146 for HFC 134a, respectively.

Parts a and b of Figure 3 show saturated liquid density deviations from the present correlations for HCFC 123 and HFC 134a, respectively. Present results for HCFC 123 show excellent agreement with available measurements by Yokoyama et al. (*2*) and by Tanikawa et al. (*3*). Present results for HFC 134a show excellent agreement with our previous measurements by Piao et al. (*4*) at Keio University but a systematic difference by about 0.2% is found between the present results and other measurements by Wilson et al. (*5*) and by Yokoyama et al. (*2*). Such an observed difference may be considered due to the different sample purities and/or isomer compositions.

Parts a and b of Figure 4 show the present results of compressed liquid isotherms and saturated liquid curves for HCFC 123 and HFC 134a, respectively. Circle and triangle symbols are saturated liquid data, whereas squares and pentagons are compressed liquid data. The saturated liquid curves were calculated by the present correlations with the aid of Piao's vapor pressure correlations (*4*, *6*), and isotherms were calculated by Kumagai's Tait equations (*7*). Present vapor pressure measurements agree with others (*4*–*6*) with the maximum deviations of −12 kPa at 350 K for HCFC 123 and of +6 kPa at 280 K for HFC 134a, respectively. Kumagai's Tait equation represents the present compressed liquid *PVT* data very well.

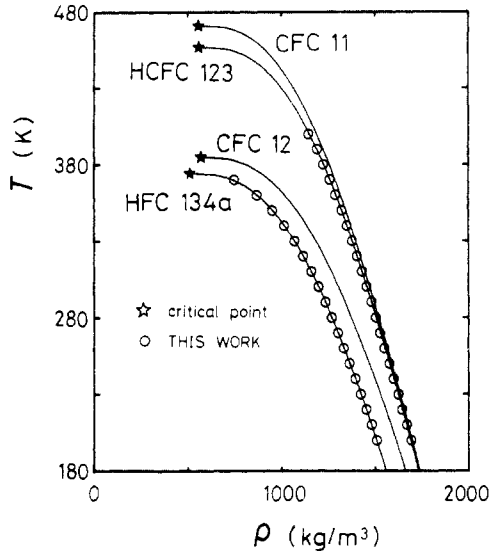

Figure 5. Comparison of saturated liquid densities of HCFC 123, HFC 134a, CFC 11, and CFC 12.

The present saturated liquid densities and present correlations for HCFC 123 and HFC 134a are compared with Okada's correlations (*1*) for CFC 11 and CFC 12 in Figure 5. Saturated liquid density of HCFC 123 differs by around 41 kg/m^3 (3.6%) from that of CFC 11 at 400 K and is closer to that of CFC 11 at lower temperatures, e.g., 4.4 kg/m^3 (0.3%) at 200 K. Saturated liquid density of HFC 134a is smaller than that of CFC 12 by about 100 kg/m^3 except in the critical region.

Acknowledgment

We are indebted to the National Research Laboratory of Metrology, Ibaraki, Japan, for the calibration of the thermometer, to the Shin'etsu Chemicals Co. Ltd., Tokyo, for furnishing the silicone oil, and to Nichiasu Co. Ltd., Tokyo, for furnishing the insulating materials. The assistance of Naoyuki Sezaki, who designed the present apparatus, of Katsuhiko Kumagai, who constructed the apparatus, and of Akira Ogino, who made all the experiments with the present authors, is gratefully acknowledged. And, Tuneyuki Hagiwara who assembled the peak detector is also gratefully acknowledged.

Literature Cited

(1) Okada, M.; Uematsu, M.; Watanabe, K. *J. Chem. Thermodyn.* **1986**, *18*, 527-543.
(2) Yokoyama, T.; Takahashi, S. Preprints of the 29th High Pressure Conference, Japan, 1988; pp 116-117.
(3) Tanikawa, S.; Kabata, Y.; Sato, H.; Watanabe, K. *Proc. Asian Thermophys. Conf.* **1989**, *2*, 513-518.
(4) Piao, C. C.; Sato, H.; Watanabe, K. *ASHRAE Trans.*, in press.
(5) Wilson, D. P.; Basu, R. S. *ASHRAE Trans.* **1988**, *94* (2), 2095-2118.
(6) Piao, C. C.; Sato, H.; Watanabe, K. *Proceedings of the 1988 Japanese Association of Refrigeration Annual Conference*; 1988; pp 5-8.
(7) Kumagai, A. *Nippon Kagakukaishi* **1984**, *7*, 1079-1082.
(8) Kabata, Y.; Tanikawa, S.; Uematsu, M.; Watanabe, K. *Int. J. Thermophys.* **1989**, *10* (3), 605-615.

Received for review May 23, 1989. Accepted January 16, 1990. We are also indebted to the grant by Tokyo Electric Power Co. Ltd., Tokyo. We are indebted to the Grant-in-Aid for Scientific Research Fund in 1989 (Project No. 01603022 and 01790369) by the Ministry of Education, Science and Culture, Japan.

Equilibrium Phase Compositions, Phase Densities, and Interfacial Tensions for CO_2 + Hydrocarbon Systems. 6. CO_2 + *n*-Butane + *n*-Decane

Narayana Nagarajan,† Khaled A. M. Gasem, and Robert L. Robinson, Jr.*
School of Chemical Engineering, Oklahoma State University, Stillwater, Oklahoma 74078

Experimental vapor-liquid equilibrium phase compositions, phase densities, and interfacial tensions are presented for the ternary system CO_2 + *n*-butane + *n*-decane at 160 °F. Measurements were made on a mixture of constant overall molar composition of 90.2% CO_2, 5.9% *n*-C_4, 3.9% *n*-C_{10} at pressures from 1310 psia to a near-critical dew point state at 1675 psia. Additional data were obtained at a constant pressure of 1600 psia. The measured phase compositions are in agreement with the data of Metcalfe and Yarborough. The phase densities and interfacial tensions represent data not previously available in the literature.

Introduction

This work is a part of our continuing studies (*1-3*) of phase behavior and interfacial tension (IFT) in mixtures of CO_2 with a series of hydrocarbon solvents, including pure and mixed hydrocarbons and reservoir oils. The present study of the ternary system formed by CO_2, *n*-butane, and *n*-decane complements our earlier work on the binary systems CO_2 + *n*-butane (*1*) and CO_2 + *n*-decane (*2*).

The data from our studies provide a basis for developing/testing models for the prediction of phase behavior and IFT in these systems. The ternary data from this work provide an opportunity to test the ability of models, containing parameters optimized to describe binary data, to describe mixtures containing a larger number of components. As such, these tests form a logical bridge between binary systems and real-oil mixtures.

Experimental Method

The experimental facility and procedures have been described in detail previously (*1*). Procedures employed in the present study were identical with those used in our CO_2 + *n*-decane (*2*) studies. The only difference in operating procedures involved the technique for charging materials to the apparatus, as described below.

Our primary objective was to study the effect of pressure on the phase behavior at constant temperature and, in particular, to include the near-critical region where IFT approaches zero. (This is of particular interest in enhanced oil recovery applica-

* To whom correspondence should be addressed.
† Present address: Mobil Research and Development Corp., P.O. Box 819047, Dallas, TX 75381-9047.

0021-9568/90/1735-0228$02.50/0